Assessment of WENO Methods with Shock-Confining Filtering for LES of Compressible Turbulence

Nathan E. Grube,* Ellen M. Taylor,† and M. Pino Martín‡
Princeton University, Princeton, NJ 08544 USA

Large-eddy simulations (LES) rely on a spatial filter to separate turbulent scales into resolved scales and scales to be modeled, and the majority of modern closure models themselves involve filtering operations. The uniform application of discrete linear filters can create new extrema in the vicinity of flow discontinuities. These new extrema can lead to spurious oscillations and to antiphysical features such as negative pressures. This is similar to the difficulty encountered when using a high-order-accurate linear finite difference scheme for convective terms in a shock-containing flow. In the case of the convective terms, many shock-capturing methods have been devised to provide physically correct solutions free from spurious oscillations. For example, weighted essentially non-oscillatory (WENO) schemes adapt their numerical stencils in the vicinity of a shock to avoid interpolation across it. In this paper, we propose a "shock-confining" filter (SCF) that adapts to avoid filtering across discontinuities. We present a method for constructing an SCF from a general linear filter and assess its performance both in traditional LES models, as exemplified by the dynamic mixed model (DMM), and in mathematical models, as exemplified by the approximate deconvolution model (ADM). Numerical studies of the shocktube problem show that the SCF greatly improves the behavior of the ADM by eliminating spurious oscillations near discontinuities. Simulations of decaying compressible isotropic turbulence show that the SCF gives behavior for the DMM and ADM that is at least comparable to, and in some way better than, the behavior of DMM with linear filtering. Although the best results for the decaying turbulence come from the ADM with relaxation, we do not consider this to be a significant drawback to the SCF because the SCF enables the ADM to behave qualitatively correctly in flows where the ADM solution would otherwise exhibit large antiphysical oscillations. Shock-confining filtering in conjunction with ADM improves the prediction of gasdynamics effects without significantly altering the prediction of turbulence; therefore, we conclude that it holds promise for LES of shock/turbulence interaction problems.

I. Introduction

Most turbulent flows contain such a large range of length and time scales that direct numerical simulation (DNS) of the governing equations is prohibitively expensive. One alternative is large-eddy simulation (LES), in which a spatial filter separates the flow scales into large, resolved scales that are computed directly, and smaller, unresolved scales, the effects of which must be modeled. The filtering into resolved and unresolved scales may be accomplished either by explicitly applying a known filter or by allowing the truncation effects of the grid and finite differene scheme to filter the flow implicitly. In both implicitly and explicitly filtered LES,

*Graduate Student, Mechanical and Aerospace Engineering Department, Princeton University, AIAA Member.
†Research Associate, Mechanical and Aerospace Engineering Department, Princeton University, AIAA Student Member.
‡Assistant Professor, Mechanical and Aerospace Engineering Department, Princeton University, AIAA Senior Member.

most popular models for the unclosed terms involve numerically explicit filtering operations. For example, the dynamic model of Germano et al.[1,2] and the the scale-similarity model (SSM) of Bardina et al.,[3] as well as the dynamic mixed model (DMM) formed by combining them,[4] use explicit filtering to isolate the smallest resolved scales of various quantities; and the approximate deconvolution model (ADM) of Stolz and Adams[5–7] uses the repeated application of an explicit filter in order to approximate the inverse of the filtering operation.

Because of the large range of length scales, turbulent flows are most efficiently simulated using high-order-accurate numerical schemes that can accurately approximate derivatives of fluctuations over a wide range of wavenumbers. However, in compressible flows containing shock waves and other discontinuities, the uniform application of high-order-accurate linear differencing schemes for approximating the spatial derivatives of the convective fluxes leads to the creation of spurious oscillations in regions where the differencing stencil crosses a discontinuity. Over time, these oscilations can grow, corrupting the solution and ultimately causing antiphysical features, such as negative temperatures, which make it impossible to proceed with the simulation. A variety of shock-capturing methods have been proposed to avoid the creation of these spurious oscillations. Among them are the essentially non-oscillatory (ENO) method[8,9] and the weighted essentially non-oscillatory (WENO) method[10,11] which measure the local smoothness of the flow and then narrow and bias their differencing stencils where needed in order to avoid high-order-accurate interpolation across discontinuities. By adapting the differencing stencil to avoid interpolation across discontinuities, these methods succeed in greatly reducing or eliminating spurious oscillations.

The thickness of a shock is typically orders of magnitude smaller than even the Kolmogorov scale in a turbulent flow, and so, in order to faithfully simulate the physics of an interaction between turbulence and a shock, the shock should remain as thin relative to the turbulence as possible. Most shock-capturing schemes require about four grid points to resolve a shock. Therefore, even without filtering, shocks are already numerically smeared in a DNS, and even more so in an LES.

Large-eddy simulation of a shock-containing flow presents a fundamental conceptual dilemma with regard to filtering in space: on the one hand, we want to remove small turbulent scales from the solution in order to model them and thus lower the computational cost; on the other hand, discontinuities such as shocks are already numerically smeared. Furthermore, shocks are governed by principles of gasdynamics, and we do not seek to model them with our closure models that are based on the physics of turbulence. If we simply apply a linear filter in a turbulence model, the difference in properties across a shock may be incorrectly interpretted by the turbulence model as a large fluctuation due to turbulence. Based on these conceptual considerations, we desire not to filter shocks.

Another consideration in filtering shock-containing flows is a more practical one, similar to that faced in computing the Navier-Stokes convective terms. The discrete linear filters used in traditional LES rely on data from a stencil of fixed width centered about the grid point of interest. Part of the filter stencil may lie across the shock; and, in general, filtering across a shock will cause smearing of the shock and/or the creation of new maxima and minima on either side of the shock. In fact, in a concurrent paper, Taylor et al.[12] show that the effect of linear filtering on DNS data from an interaction between a shock wave and compressible isotropic tubulence can produce instances of negative temperature. Thus, in some sense, the traditional LES of such a flow might be doomed from the start, since its “exact” or “target” solution has antiphysical aspects. Filtering across discontinuities can also cause negative temperatures to develop in ADM simulations (including non-turbulent ones such as the shocktube problem). Although the introduction of a relaxation regularization term[6,7] helps to avoid negative temperatures, it still does not give relief from qualitatively incorrect oscillations.

Therefore, there are both conceptual and practical reasons why we wish to avoid filtering across shocks. (W)ENO methods for computing the convective terms devote significant computational effort to measuring the local smoothness of the flow in order to determine how to adapt the difference stencil at each point. We propose an adaptive shock-confining filter (SCF) which seeks to filter turbulent scales in smooth regions according to a known linear filter function, while at the same time affecting discontinuities as little as possible and keeping them confined to as few grid points as is allowed by the underlying shock-capturing scheme. Because the SCF is used in conjunction with a WENO scheme, the smoothness measurement from the convective terms can be reused, and there is little increase in computational cost due to measuring smoothness.

The purpose of this paper is to assess the suitability of shock-confining filtering for LES of shock-conatining flows, particularly in the context of ADM simulations, but also in the context of traditional LES. Section II reviews the governing conservation equations as well as the terms to be modeled in both traditional LES, as exemplified by the dynaimc mixed model, and mathematical LES, as exemplified by the approximate deconvolution method. Section III discusses filtering for LES, both traditional linear filters and SCF. A method is presented for constructing an SCF from a general linear filter such that the SCF retains the filter properties necessary for a qualitatively correct solution of gasdynamics problems. Section IV presents numerical simulations that demonstrate the behavior of the SCF in simulations of gasdynamics flows, as exemplified by the shocktube problem, and in turbulent shocklet-containing flows, as exemplified by decaying isotropic turbulence. Section V presents general conclusions about shock-confining filters.

II. Compressible Large-eddy Simulations

The temporal evolution of a fluid flow is governed by conservation laws for mass, momentum and energy, which we will collectively refer to as the Navier-Stokes equations. They can be written as:

$$\frac{\partial \rho}{\partial t} + \frac{\partial}{\partial x_j}(\rho u_j) = 0 \tag{1a}$$

$$\frac{\partial}{\partial t}(\rho u_i) + \frac{\partial}{\partial x_j}(\rho u_i u_j + p\delta_{ij} - \sigma_{ij}) = 0 \tag{1b}$$

$$\frac{\partial}{\partial t}(E) + \frac{\partial}{\partial x_j}\left[(E+p)u_j + q_j - \sigma_{ij}u_i\right] = 0 \tag{1c}$$

where ρ is density, u_j is velocity in the x_j direction, p is pressure, δ_{ij} is the Kronecker delta, $E = \rho c_v T + \frac{1}{2}\rho u_k u_k$ is total energy, T is temperature, $\sigma_{ij} = 2\mu S_{ij}(U) - \frac{2}{3}\mu\delta_{ij}S_{kk}(U)$ is the viscous stress tensor, μ is viscosity, $S_{ij}(U) = \frac{1}{2}\left(\frac{\partial u_j}{\partial x_i} + \frac{\partial u_i}{\partial x_j}\right)$ is the strain rate tensor, $q_j = -k\frac{\partial T}{\partial x_j}$ is the heat flux, and k is thermal conductivity.

To close the system, we use the perfect gas equation of state $p = \rho RT$; a power law for viscosity (in air) $\mu = \mu_{\text{ref}}(T/T_{\text{ref}})^p$, where $\mu_{\text{ref}} = 1.789 \times 10^{-5} kg/m \cdot s$, $T_{\text{ref}} = 288.2K$, and $p = 0.76$; and an assumption of proportionality between thermal conductivity and viscosity $k = (19/4)R\mu$ (for a diatomic gas).

Most turbulent flows contain such a large range of length and time scales that direct numerical simulation (DNS) of the governing equations is prohibitively expensive. Instead, a spatial filtering operation is employed to separate the flow scales into large, resolved scales that can be computed directly, and smaller, unresolved scales, the effects of which must be modeled. Let us define a low-pass filter in terms of a convolution: $\bar{u} = \int G(\vec{x},\vec{y})u(\vec{y})d\vec{y} \equiv G * u$. In order to simplify the analysis of compressible flows, it is also useful to define a Favre (density weighted) filter as $\tilde{f} = \overline{\rho f}/\bar{\rho}$.

A brief note about terminology is in order. Large-eddy simulations can be categorized as either implicitly filtered or explicitly filtered. Implicitly filtered LES relies on the grid truncation and differencing errors to effectively provide a low-pass filter of unknown shape. Explicitly filtered LES uses a known low-pass filter with a cutoff at lower wavenumbers than the grid Nyquist limit. Thus, in implicit LES, the terms subgrid- and subfilter-scale (SGS and SFS) are interchangeable. In explicit LES, we shall use "SGS" to refer to scales too small to be represented on the grid, and "SFS" to refer to scales which are representable on the grid but which are not resolved by the filter. The full unclosed or unresolved terms are the sum of the SFS and SGS parts. This paper deals with ADM and explicit LES, both of which use a filter with a cutoff at lower wavenumbers than the grid Nyquist limit, and both of which have distinct SFS and SGS terms. In analytical discussions where grid truncation and differencing have not been considered, there is no grid filter, and hence for convenience we sometimes call analytical unclosed terms SFS.

The only filtered variables that are available in LES are the filtered conserved variables, $\overline{U}$ or ($\overline{\rho}$, $\overline{\rho u}$, $\overline{\rho v}$, $\overline{\rho w}$, $\overline{E}$), which evolve according to the filtered Navier-Stokes equations. All other quantities associated with the filtered solution (e.g., primitive varables and transport coefficients) can only be approximated as functions of known filtered quantities. This is accomplished by writing an expression for the desired quantity in terms of exact conserved variables and then substituting filtered conserved variables into this definition. We denote a quantity computed in this way by a check: $f = f(U) \Rightarrow \check{f} = f(\overline{U}) \neq \overline{f}$. For example, $\overline{p} = (\gamma - 1)\left[\overline{E} - \frac{1}{2}\overline{\rho u_k u_k}\right]$ cannot be obtained exactly because $\overline{\rho u_k u_k}$ contains information from unresolved scales. We must either use a model or else use $\check{p} = (\gamma - 1)\left[\overline{E} - \frac{1}{2}\bar{\rho}\tilde{u}_k\tilde{u}_k\right]$. Note that the Favre filtered velocities $\{\tilde{u}_i\}$ could also have been written as $\{\check{u}_i\}$.

We construct governing equations for LES by applying the filter to the Navier-Stokes equation and then rearranging terms so that the left-hand side has the same operational form as the original Navier-Stokes equations but with resolved variables replacing the full variables:

$$\frac{\partial \bar{\rho}}{\partial t} + \frac{\partial}{\partial x_j}(\bar{\rho}\tilde{u}_j) = 0, \tag{2a}$$

$$\frac{\partial}{\partial t}(\bar{\rho}\tilde{u}_i) + \frac{\partial}{\partial x_j}(\bar{\rho}\tilde{u}_i\tilde{u}_j + \bar{p}\delta_{ij} - \check{\sigma}_{ij}) = -\frac{\partial}{\partial x_j}\tau_{ij}, \tag{2b}$$

$$\frac{\partial}{\partial t}(\overline{E}) + \frac{\partial}{\partial x_j}\left[(\overline{E} + \bar{p})\tilde{u}_j + \check{q}_j - \check{\sigma}_{ij}\tilde{u}_i\right] = -\frac{\partial}{\partial x_j}(\gamma c_v Q_j + \frac{1}{2}J_j - D_j), \tag{2c}$$

where $\check{\sigma}_{ij} = 2\check{\mu}S_{ij}(\overline{U}) - \frac{2}{3}\check{\mu}\delta_{ij}S_{kk}(\overline{U})$ with $S_{ij}(\overline{U}) = \frac{1}{2}\left(\frac{\partial \tilde{u}_j}{\partial x_i} + \frac{\partial \tilde{u}_i}{\partial x_j}\right)$, and $\check{q}_j = -\check{k}\frac{\partial \check{T}}{\partial x_j}$.

We have neglected unclosed terms arising from the viscous stresses in the momentum equation and the heat conduction term in the energy equation. Notice that we have written the left-hand side of the momentum equations using the unknown $\overline{p}$ rather than the known $\check{p}$. The difference between these quantities, $\overline{p} - \check{p} = -\frac{(\gamma-1)}{2}\tau_{kk}$, is approximated using the model for τ_{ij}, and similarly for the unknown quantity $\widetilde{T}$ in the heat conduction term.

The terms to be closed are the SFS stresses $\tau_{ij} = \bar{\rho}(\widetilde{u_i u_j} - \tilde{u}_i\tilde{u}_j)$, the SFS heat flux $Q_j = \bar{\rho}(\widetilde{u_j T} - \tilde{u}_j\tilde{T})$, SFS diffusion of turbulent kinetic energy $J_j = \bar{\rho}(\widetilde{u_j u_k u_k} - \tilde{u}_j\widetilde{u_k u_k})$, and the SFS viscous diffusion of energy $D_j = \bar{\rho}(\overline{\sigma_{ij} u_i} - \tilde{\sigma}_{ij}\tilde{u}_i)$.

Martín et al.[13] perform an *a priori* analysis of the unclosed terms in the energy budget for decaying isotropic turbulence with $Re_\lambda = \rho_{\text{avg}}u'_{\text{rms}}\lambda/\mu = 50$ and $M_t = q/a_{\text{avg}} = 0.52$ where q is the root-mean-square fluctuating velocity magnitude and a_{avg} is the average speed of sound. They find that the most important SFS term in the energy equation is the heat flux Q_j and that the contribution from the SFS turbulent diffusion J_j is smaller by approximately a factor of two. The contribution from SFS viscous diffusion D_j is approximately an order of magnitude smaller than that from Q_j. We therefore choose to neglect D_j. We also neglect J_j, in part because its effect is smaller than that of Q_j and in part because models for J_j are less well-developed.

II.A. Traditional LES Models

II.A.1. Dynamic Smagorinsky Model

In traditional compressible LES, we must model the retained unclosed terms τ_{ij} and Q_j. The simplest approach is an eddy diffusivity term for transport of momentum and heat, such as the Smagorinsky[14] model along with a turbulent Prandtl number:

$$\tau_{ij} - \frac{\delta_{ij}}{3}\tau_{kk} \approx C\alpha_{ij}, \tag{3}$$

$$Q_j \approx -\frac{C}{Pr_{\mathrm{turb}}}\alpha_j^T, \tag{4}$$

where

$$\alpha_{ij} = -2\overline{\Delta}^2\overline{\rho}\left|S(\overline{U})\right|\left(S_{ij}(\overline{U}) - \frac{\delta_{ij}}{3}S_{kk}(\overline{U})\right), \tag{5}$$

$$\alpha_j^T = \overline{\Delta}^2\overline{\rho}\left|S(\overline{U})\right|\left(\frac{\partial \widetilde{T}}{\partial x_j}\right), \tag{6}$$

$|S_{ij}| = \sqrt{2S_{ij}S_{ij}}$, $\overline{\Delta}$ is the cutoff lengthscale of the filter, and C and Pr_{turb} are model parameters.

We can dynamically compute the model parameters[1,2,15] using a self-similarity assumption between the flow filtered at the $\overline{\cdot}$ level and the flow filtered a second time using a test filter $\widehat{\cdot}$ such that the cutoff lengthscale of the composite filter $\widehat{\overline{\cdot}}$ is twice that of the original filter $\overline{\cdot}$ alone. The test filtering introduces new SFS terms at the test filter level:

$$T_{ij} = \widehat{\overline{\rho}}(\breve{\widetilde{u_i u_j}} - \breve{\widetilde{u}}_i\breve{\widetilde{u}}_j), \tag{7}$$

$$\mathbb{Q}_j = \widehat{\overline{\rho}}\left(\breve{\widetilde{Tu_j}} - \breve{\widetilde{T}}\breve{\widetilde{u}}_j\right), \tag{8}$$

where $\breve{\widetilde{f}} \equiv \widehat{\overline{\rho f}}/\widehat{\overline{\rho}}$ is the Favre filter associated with the composite filter $\widehat{\overline{\cdot}}$. The unclosed stresses at the test filtered level can be related to those at the LES filtered level using the Germano identity:

$$\mathcal{L}_{ij} = T_{ij} - \widehat{\tau_{ij}}, \tag{9}$$

where

$$\mathcal{L}_{ij} \equiv \widehat{\left(\frac{\overline{\rho u_i}\;\overline{\rho u_j}}{\overline{\rho}}\right)} - \frac{\widehat{\overline{\rho u_i}}\;\widehat{\overline{\rho u_j}}}{\hat{\overline{\rho}}} \tag{10}$$

is the "resolved" part of the SFS stress at the $\widehat{\overline{(.)}}$ level and can be computed from known quantities. (Note that the test filter acts on the entire first term, not only the numerator.) Applying the Smagorinsky model to the stresses at both filter levels in (9) yields:

$$\mathcal{L}_{ij} = C\beta_{ij} - \widehat{C\alpha_{ij}}, \tag{11}$$

where

$$\beta_{ij} = -2\widehat{\overline{\Delta}}^2\widehat{\overline{\rho}}\left|S(\widehat{\overline{U}})\right|\left(S_{ij}(\widehat{\overline{U}}) - \frac{\delta_{ij}}{3}S_{kk}(\widehat{\overline{U}})\right), \tag{12}$$

and $S_{ij}(\widehat{\overline{U}}) = \frac{1}{2}\left(\frac{\partial \breve{\widetilde{u}}_j}{\partial x_i} + \frac{\partial \breve{\widetilde{u}}_i}{\partial x_j}\right)$. Assuming that the parameter C can be pulled outside of the test filter operation, we can solve for C:

$$C = \frac{\langle \mathcal{L}_{ij} M_{ij}\rangle}{\langle M_{lk} M_{lk}\rangle}, \tag{13}$$

where

$$M_{ij} = \beta_{ij} - \widehat{\alpha_{ij}}. \tag{14}$$

The angle brackets indicate averaging over homogeneous directions, which, it is hoped, mitigates the incorrectness of pulling C out of the test filter operation. After averaging, the numerator is clipped to zero to eliminate any negative values.

A similar procedure yields a dynamic prediction for the turbulent Prandtl number:

$$\frac{Pr_{\mathrm{turb}}}{C} = \frac{\left\langle M_k^T M_k^T \right\rangle}{\left\langle \mathcal{L}_j^T M_j^T \right\rangle} \tag{15}$$

where

$$\mathcal{L}_j^T = \left(\frac{\widehat{\overline{\rho T}\;\overline{\rho u_j}}}{\overline{\rho}} \right) - \frac{\widehat{\overline{\rho T}}\;\widehat{\overline{\rho u_j}}}{\hat{\overline{\rho}}}, \tag{16}$$

$$M_j^T = \beta_j^T - \widehat{\alpha_j^T}, \tag{17}$$

and

$$\beta_j^T = \widehat{\overline{\Delta}}^{\,2} \widehat{\overline{\rho}} \left| S(\widehat{\overline{U}}) \right| \left(\frac{\partial \breve{\tilde{T}}}{\partial x_j} \right). \tag{18}$$

II.A.2. Dynamic Mixed Model

The dynamic Smagorinsky model adds an appropriate amount of global dissipation to the flow; however, the model predictions correlate poorly in space with the exact SFS terms in *a priori* studies using DNS data. The scale-similarity model (SSM) of Bardina et al.[3] correlates much better. This model is of the form:

$$\tau_{ij} \approx A_{ij} \equiv \overline{\rho} \left(\widetilde{\tilde{u}_i \tilde{u}_j} - \tilde{\tilde{u}}_i \tilde{\tilde{u}}_j \right). \tag{19}$$

The SSM accurately represents the spatial structure of the SFS stresses in *a priori* studies, but it is insufficiently dissipative. Speziale et al.[16] proposed a mixed model composed of a linear combination of an eddy diffusivity model and the SSM. A dynamic mixed model (DMM) was proposed by Vreman et al.[4] The DMM combines the improved spatial correlation of the SSM with the proper global dissipation of the dynamic Smagorinsky model.

This study will take the one-coefficient dynamic mixed model as reported in Martín et al.[13] as representative of traditional LES models. This model can be written:

$$\tau_{ij} \approx C\alpha_{ij} + A_{ij} \tag{20}$$

Because the eddy diffusivity term now models only the difference between the unclosed term τ_{ij} and the SSM term A_{ij}, the dynamic coefficient is calculated from

$$C = \frac{\langle \mathcal{L}_{ij} M_{ij} \rangle - \langle N_{ij} M_{ij} \rangle}{\langle M_{lk} M_{lk} \rangle}, \tag{21}$$

where

$$N_{ij} = B_{ij} - \widehat{A_{ij}} \tag{22}$$

and

$$B_{ij} = \hat{\overline{\rho}} \left(\breve{\widetilde{\breve{\tilde{u}}_i \breve{\tilde{u}}_j}} - \breve{\tilde{\breve{\tilde{u}}}}_i \breve{\tilde{\breve{\tilde{u}}}}_j \right) \tag{23}$$

is the SSM term associated with the test filter level.

Similarly, the SFS heat flux is modeled as:

$$Q_j \approx -\frac{C}{Pr_{\mathrm{turb}}} \alpha_j^T + A_j^T, \tag{24}$$

where

$$A_j^T = \overline{\rho} \left(\widetilde{\tilde{T} \tilde{u}_j} - \tilde{\tilde{T}} \tilde{\tilde{u}}_j \right), \tag{25}$$

and the turbulent Prandtl number is computed from

$$\frac{Pr_{\text{turb}}}{C} = \frac{\left\langle M_k^T M_k^T \right\rangle}{\left\langle \mathcal{L}_j^T M_j^T \right\rangle - \left\langle N_j^T M_j^T \right\rangle}, \tag{26}$$

where

$$N_j^T = B_j^T - \widehat{A_j^T} \tag{27}$$

and

$$B_j^T = \widehat{\overline{\rho}} \left(\widetilde{\breve{\breve{T}}\breve{\breve{u}}_j} - \breve{\breve{T}}\breve{\breve{u}}_j \right). \tag{28}$$

II.B. Approximate Deconvolution Method

Another LES closure method is the Approximate Deconvolution Method (ADM) of Stolz and Adams.[5] In this method, the spatially filtered flow solution is approximately defiltered using an iterative application of G in an algorithm proposed by van Cittert.[17] As an approximate inverse to a filter G, we define $Q_N = \sum_{i=0}^{N} (I - G)^i \approx G^{-1}$. Figure 1 shows transfer functions for the simple tophat filter (56) and for the composition of the tophat and its approximate inverse as given by five terms in van Cittert's deconvolution method.

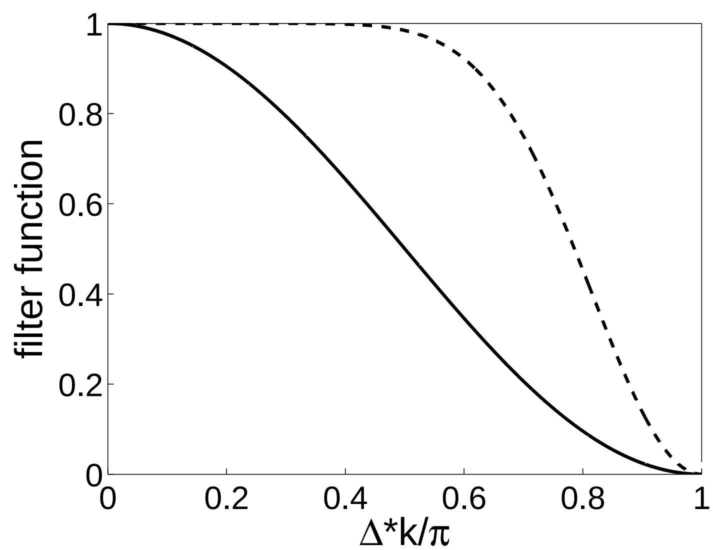

Figure 1. Filter functions for simple tophat filter (———) and composition (– – – –) of simple tophat filter with its approximate inverse as given by five terms in van Cittert's deconvolution method.

The resulting defiltered data $U^\star = Q_N * \overline{U} = Q_N \circ G * U$ are used as an approximation to the exact (unfiltered) flow quantities and are substituted directly into the inviscid flux terms on the left-hand side of the Navier-Stokes equations.

The Navier-Stokes equations can be written in terms of fluxes as:

$$\frac{\partial}{\partial t}\mathbf{U} + \frac{\partial}{\partial x_j}\mathbf{E}_j(\mathbf{U}) + \frac{\partial}{\partial x_j}\mathbf{E}_j^{\text{visc}}(\mathbf{U}) = 0 \tag{29}$$

where

$$\mathbf{U} = \begin{pmatrix} \rho \\ \rho u_1 \\ \rho u_2 \\ \rho u_3 \\ E \end{pmatrix} \tag{30}$$

is the vector of conserved variables,

$$\mathbf{E}_j(\mathbf{U}) = \begin{pmatrix} \rho u_j \\ \rho u_1 u_j + p\delta_{1j} \\ \rho u_2 u_j + p\delta_{2j} \\ \rho u_3 u_j + p\delta_{3j} \\ (E+p)u_j \end{pmatrix} \tag{31}$$

is the vector of inviscid fluxes in the x_j direction, and

$$\mathbf{E}_j^{\text{visc}}(\mathbf{U}) = \begin{pmatrix} 0 \\ -\sigma_{1j} \\ -\sigma_{2j} \\ -\sigma_{3j} \\ q_j - \sigma_{ij}u_i \end{pmatrix} \tag{32}$$

is the vector of viscous fluxes in the x_j direction. We will neglect the unclosed terms arising from the viscous fluxes. Then the LES governing equations can similarly be written

$$\frac{\partial}{\partial t}\overline{\mathbf{U}} + \frac{\partial}{\partial x_j}\mathbf{E}_j(\overline{\mathbf{U}}) + \frac{\partial}{\partial x_j}\mathbf{E}_j^{\text{visc}}(\overline{\mathbf{U}}) = -\frac{\partial}{\partial x_j}\mathbf{T}_j^{\text{full}}, \tag{33}$$

where

$$\mathbf{T}_j^{\text{full}} \equiv \left[\overline{\mathbf{E}_j(\mathbf{U})} - \mathbf{E}_j(\overline{\mathbf{U}})\right]. \tag{34}$$

Traditional SFS models tend to model the full unresolved quantity $\mathbf{T}^{\text{full}}$. In ADM, we compute approximately defiltered variables $\mathbf{U}^\star$, which approximately represent the resolved scales plus the scales that are between the filter cutoff wavenumber and the Nyquist cutoff wavenumber for the grid. In the context of ADM, we call such scales sub-filter scales (SFS) to distinguish them from subgrid scales (SGS) that are smaller than the Nyquist limit for the grid and cannot be represented at all. The full unclosed terms may be decomposed into SFS and SGS parts:

$$\mathbf{T}_j^{\text{full}} = \underbrace{\overline{\mathbf{E}_j(\mathbf{U})} - \overline{\mathbf{E}_j(\mathbf{U}^\star)}}_{\mathbf{T}_j^{SGS}} + \underbrace{\overline{\mathbf{E}_j(\mathbf{U}^\star)} - \mathbf{E}_j(\overline{\mathbf{U}})}_{\mathbf{T}_j^{SFS}}. \tag{35}$$

The second term in $\mathbf{T}^{\text{SFS}}$ is expressed in terms of known, filtered variables. It can be computed exactly. In fact, it cancels with the convective term on the left-hand side. The first term in $\mathbf{T}^{\text{SFS}}$ is also known once $\mathbf{U}^\star$ has been calculated, so it is moved to the left-hand side, leaving only $\mathbf{T}^{\text{SGS}}$ to be modeled:

$$\frac{\partial}{\partial t}\overline{\mathbf{U}} + \frac{\partial}{\partial x_j}\overline{\mathbf{E}_j(\mathbf{U}^\star)} + \frac{\partial}{\partial x_j}\mathbf{E}_j^{\text{visc}}(\overline{\mathbf{U}}) = -\frac{\partial}{\partial x_j}\mathbf{T}_j^{SGS}. \tag{36}$$

II.B.1. Regularization by Relaxation

Stolz et al.[6,7] model the dissipative effect of the SGS terms using relaxation terms with dynamic coefficients to keep the energy content of the small scales approximately constant. The resulting equations can be written:

$$\frac{\partial}{\partial t}\overline{\mathbf{U}} + \frac{\partial}{\partial x_j}\overline{\mathbf{E}_j(\mathbf{U}^\star)} + \frac{\partial}{\partial x_j}\mathbf{E}_j^{\text{visc}}(\overline{\mathbf{U}}) = -\mathbf{X}, \tag{37}$$

where

$$\mathbf{X} = \begin{pmatrix} \chi_\rho[\overline{(\rho)} - \overline{(\rho)^\star}] \\ \chi_{\rho u}[\overline{(\rho u_1)} - \overline{(\rho u_1)^\star}] \\ \chi_{\rho u}[\overline{(\rho u_2)} - \overline{(\rho u_2)^\star}] \\ \chi_{\rho u}[\overline{(\rho u_3)} - \overline{(\rho u_3)^\star}] \\ \chi_E[\overline{(E)} - \overline{(E)^\star}] \end{pmatrix} = \begin{pmatrix} \chi_\rho(I - Q_N \star G) \star (\rho) \\ \chi_{\rho u}(I - Q_N \star G) \star (\rho u_1) \\ \chi_{\rho u}(I - Q_N \star G) \star (\rho u_2) \\ \chi_{\rho u}(I - Q_N \star G) \star (\rho u_3) \\ \chi_E(I - Q_N \star G) \star E \end{pmatrix}, \tag{38}$$

where χ_ρ, $\chi_{\rho u}$, and χ_E are dynamic relaxation parameters, and the operation $(I - Q_N * G)$ is used to isolate the smallest scales in the flow that can be represented by the grid. Details of the dynamic procedure for determining the parameters χ_ρ, $\chi_{\rho u}$, and χ_E can be found in Stolz et al.[6,7]

Regularization by relaxation has been used successfully for moderately supersonic Mach numbers. However, the removal of small scales has the effect of creating Gibbs-like overshoots and oscillations near discontinuities; in Section IV.A we see that the relaxation regularization fares rather poorly in the case of a shocktube. As the Mach number increases, discontinuities grow, and the problems affecting ADM with relaxation can be expected to become more severe. Here, with the eventual goal of reaching hypersonic Mach numbers, we use a dynamic eddy viscosity model along with a dynamic turbulent Prandtl number to account for the effect of the SGS scales.

II.B.2. Regularization by Functional Modeling

The relaxation approach to regularization of the ADM equations did not use any phenomenological knowledge of the transfer of energy from represented scales to subgrid scales. Here we propose a model based on the assumption that such a transfer is carried out by a turbulent gradient diffusion process. A dynamic Smagorinksy model is derived similarly to the eddy diffusivity part of the traditional dynamic mixed model, except that here the ADM treatment for $\mathbf{T}_j^{SFS}$ takes the place of Bardina's scale-similarity model.

The SGS terms in the ADM governing equations can be written:

$$\mathbf{T}_j^{SGS} = \begin{pmatrix} \mathcal{R}_j \\ \mathcal{T}_{1j} + \delta_{1j}\mathcal{P} \\ \mathcal{T}_{2j} + \delta_{2j}\mathcal{P} \\ \mathcal{T}_{3j} + \delta_{3j}\mathcal{P} \\ \gamma c_v \mathcal{Q}_j + \frac{1}{2}\mathcal{J}_j \end{pmatrix}, \tag{39}$$

where the unclosed terms for the ADM equations are:

$$\mathcal{R}_j = \overline{(\rho u_j)} - \overline{(\rho u_j)^\star} \tag{40}$$

$$\mathcal{T}_{ij} = \overline{\rho u_i u_j} - \overline{(\rho u_i)^\star (\rho u_j)^\star / \rho^\star} \tag{41}$$

$$\mathcal{P} = (\gamma - 1)\left[\overline{E} - \overline{E^\star}\right] - \frac{1}{2}\mathcal{T}_{kk} \tag{42}$$

$$\mathcal{Q}_j = \overline{\rho u_j T} - \overline{(\rho u_j)^\star \check{T}^\star} \tag{43}$$

$$\mathcal{J}_j = \overline{\rho u_k u_k u_j} - \overline{(\rho u_k)^\star (\rho u_k)^\star (\rho u_j)^\star / (\rho^\star)^2}. \tag{44}$$

Note that no nonlinearities (with respect to the conserved variables) appear in $\mathcal{R}_j$ or in the first bracketed term of $\mathcal{P}$. We make the simplifying assumption that these are zero. The difference between a variable ϕ and its approximately defiltered couterpart $\phi^\star$ is confined to lengthscales below the Nyquist cutoff for the grid and those just above it where the deconvolution procedure cannot reconstruct the information in a reasonable number of iterations. These lengthscales in question are either completely missing from $\overline{\phi}$ (in the case of subgrid scales) or highly attenuated due to the fact that $\hat{G}(k) \to 0$ as $k \to k_{\mathrm{Nyquist}}$. Thus, there is very little difference between $\overline{\phi}$ and $\overline{\phi^\star}$, especially for filters where $d\hat{G}(k)/dk \to 0$ as $k \to k_{\mathrm{Nyquist}}$. This is true of the filters considered in this paper.

As in the DMM case, here we model only the SGS stresses $\mathcal{T}_{ij}$ and the SGS heat flux $\mathcal{Q}_j$. It seems plausible that, in analogy to traditional LES, these are the most important terms, but *a priori* studies of DNS data should be carried out to verify this assumption.

To derive a dynamic model, we again apply a test filter to the solution. We use a superscript circle $(\cdot)^\circ$ to denote a variable that has been defiltered with respect to the composite filter $\widehat{\overline{\cdot}}$. The SGS stresses with respect to the composite filter are

$$\mathbb{T}_{ij} = \widehat{\overline{\rho u_i u_j}} - \overline{\widehat{(\rho u_i)^\circ (\rho u_j)^\circ / \rho^\circ}}. \tag{45}$$

The ADM version of Germano's identity is then

$$\mathcal{L}_{ij}^{\mathrm{ADM}} = \mathbb{T}_{ij} - \widehat{\mathcal{T}}_{ij}, \tag{46}$$

where

$$\mathcal{L}_{ij}^{\mathrm{ADM}} = \overline{\widehat{(\rho u_i)^\star (\rho u_j)^\star / \rho^\star}} - \overline{\widehat{(\rho u_i)^\circ (\rho u_j)^\circ / \rho^\circ}}. \tag{47}$$

Applying the eddy viscosity model at the two filter levels yields

$$\mathcal{L}_{ij}^{\mathrm{ADM}} = C\beta_{ij} - \widehat{C\alpha_{ij}}, \tag{48}$$

where α_{ij} and β_{ij} are as defined for the DMM in Section II.A.2. Solving for C yields

$$C = \frac{\left\langle \mathcal{L}_{ij}^{\mathrm{ADM}} M_{ij} \right\rangle}{\langle M_{lk} M_{lk} \rangle}, \tag{49}$$

where M_{ij} is as defined above. A similar procedure for the SGS heat flux yields:

$$\frac{Pr_{\mathrm{turb}}}{C} = \frac{\left\langle M_k^T M_k^T \right\rangle}{\left\langle \mathcal{L}_j^{\mathrm{ADM},\ T} M_j^T \right\rangle} \tag{50}$$

where

$$\mathcal{L}_{ij}^{\mathrm{ADM},\ T} = \overline{\widehat{(\rho u_j)^\star T^\star}} - \overline{\widehat{(\rho u_j)^\circ T^\circ}}, \tag{51}$$

and M_{ij}^T is as defined above. Finally, the SGS terms are approximated as

$$\mathcal{T}_{ij} \approx C\alpha_{ij}, \tag{52}$$

$$\mathcal{Q}_j \approx -\frac{C}{Pr_{\mathrm{turb}}}\alpha_{ij}^T. \tag{53}$$

Note that, similarly to the case of $\overline{p}$ in Section II, computing the quantities $T^\star$ and T° in general involves the modeled values for the SGS stresses $\mathcal{T}_{kk}$ and $\mathbb{T}_{kk}$ (or rather their defiltered values). The one-parameter DMM provided information about the trace of τ_{ij} due to the SSM term, even though the eddy viscosity part is traceless. However, in the case of the ADM unclosed terms, the SFS part is modeled not by an SSM term but rather by modifying the convective fluxes on the left-hand side of the equations. Therefore, no analog of the the SSM term appears in the model for $\mathcal{T}_{ij}$, and the modeled SGS stresses are traceless. For our one-parameter Smagorinsky model, then, $T^\star$ and $\check{T}^\star$ are equivalent, as are T° and $\check{T}^\circ$.

This new SGS model for compressible ADM is not a major focus of the paper, and it turns out to play very little role in the results.

III. Filtering

III.A. Traditional Discrete Filtering

Recall that we define the LES filter according to a convolution:

$$\bar{u} = \int G(\vec{x}, \vec{y}) u(\vec{y}) d\vec{y} \equiv G * u. \tag{54}$$

If the filter kernel G is chosen to have compact support, then we may write a discrete representation explicitly as

$$\overline{f}_i = \sum_{k=-N}^{N} a^k f_{i+k}; \tag{55}$$

e.g.,

$$\overline{f}_i = a^{-1} f_{i-1} + a^0 f_{i+0} + a^1 f_{i+1} = \frac{1}{4} f_{i-1} + \frac{1}{2} f_{i+0} + \frac{1}{4} f_{i+1} \tag{56}$$

is a commonly used tophat filter. We will consider the tophat filter (56) and two filters from a class of filters proposed by Vasilyev et al.[18] to minimize the commutation error between filtering and differentiation. A commutative filter with three zero-moments and a cutoff wavenumber of approximately $0.636 k_{\mathrm{Nyq.}}$ is given by the coefficients:

$$\begin{pmatrix} a_{-2} \\ a_{-1} \\ a_{\ 0} \\ a_{\ 1} \\ a_{\ 2} \end{pmatrix} = \frac{1}{16} \begin{pmatrix} -1 \\ 4 \\ 10 \\ 4 \\ -1 \end{pmatrix}. \tag{57}$$

A commutative filter with three zero-moments and a cutoff wavenumber of one-half the Nyquist limit uses the coefficients:

$$\begin{pmatrix} a_{-3} \\ a_{-2} \\ a_{-1} \\ a_{\ 0} \\ a_{\ 1} \\ a_{\ 2} \\ a_{\ 3} \end{pmatrix} = \frac{1}{32} \begin{pmatrix} -1 \\ 0 \\ 9 \\ 16 \\ 9 \\ 0 \\ -1 \end{pmatrix}. \tag{58}$$

We denote the filter (transfer) function (i.e., the Fourier transform of the filter kernel G with respect to y) as $\mathfrak{G}(k)$. The effect of applying the filter to a wave of wavenumber k is to multiply the signal by $\mathfrak{G}(k)$. If the filter is symmetric, then the filter function is real, and the filter function gives the attenuation of the signal as a function of wavenumber. We define the cutoff wavenumber to be that k such that $\mathfrak{G}(k) = 1/2$. The filter functions of the simple tophat and the commutative filters are shown in Fig 2.

In computing dynamic model coefficients, we use a test filter with a lower cutoff wavenumber. Let us call the test filter kernel H and its filter function $\mathfrak{H}(k)$. Ideally, the composite filter $H \circ G$ should have a filter

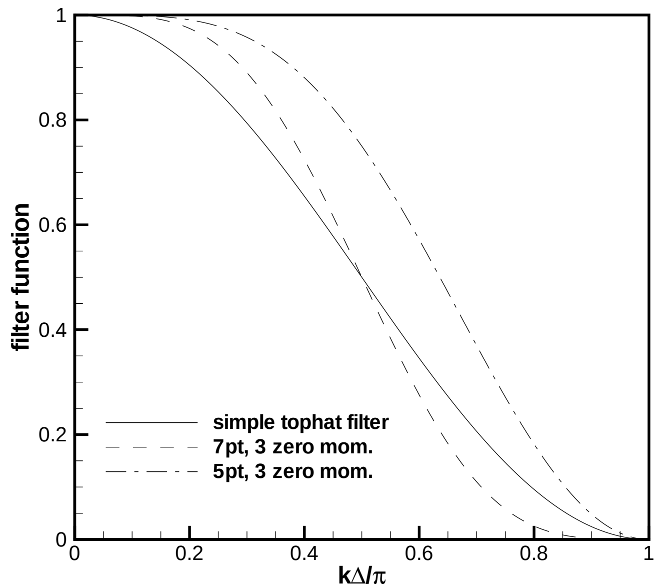

Figure 2. Filter functions for LES filters used in this paper.

function similar to $\mathfrak{G}$ in shape but of half the width. That is, $\mathfrak{H}(k/2)\mathfrak{G}(k/2) = \mathfrak{G}(k)$. In practice, we cannot obtain a test filter that gives the exact desired composite filter function. Here we use three applications of the tophat filter to approximate the correct test filter. Figure 3 plots the filter functions of the tophat filter, the test filter and the actual and ideal composite filters. The test filter based on repeated application of the tophat filter gives a composite filter function that follows the ideal composite filter function closely for low wavenumbers and tolerably well for the entire range. We could also have used the optimization procedure of Vasilyev et al.[18] to generate a test filter that gives approximately the correct composite filter function; however, such a filter would have a transfer function that crosses zero, and the approximate inversion of such a filter would fail. Since we need to defilter the test-filtered data in the propsed SGS model for ADM, we want a filter than can be inverted. The repeated application of a filter with a strictly positive filter function (up to the Nyquist wavenumber) is an easy way of generating a filter function that does not cross zero.

III.B. Shock-Confining Filters

In LES of flows with shocks, we face a fundamental dilemma with regard to filtering in space. On the one hand, we want to remove small turbulent scales from the solution in order to model them and thus lower the computational cost. On the other hand, discontinuities such as shocks are small scale flow features that are governed by gasdynamics, and we do not seek to model them with our turbulence models.

The discrete linear filters used in traditional LES rely on data from a stencil of fixed width centered about the grid point of interest. In the vicinity of shocks (or other discontinuities), part of the filter stencil may lie across a shock, and in general this filtering across a shock will cause smearing of the shock and/or the creation of new maxima and minima on either side of the shock. In order to avoid filtering across shocks, we use a shock-confining filter (SCF) which adapts its coefficients in response to the local smoothness of the flow solution. In order to determine where filter adaptation is warranted, the SCF uses information about the smoothness of the flow field that is already computed by the WENO shock-capturing scheme for the

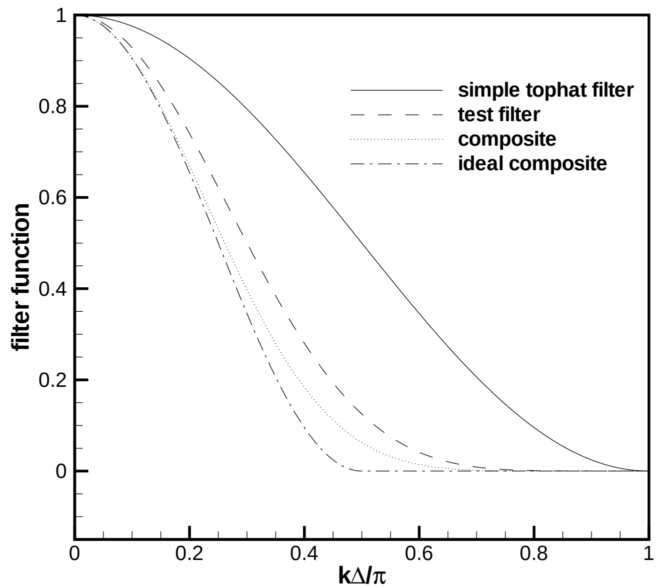

Figure 3. Filter functions for tophat LES filter, test filter based on repeated application of tophat filter, and composite of the two compared to the ideal composite filter function for the tophat.

convective terms.

Figure 4 schematically illustrates the desired behavior of an SCF: discontinuities are unaffected, but smooth regions are filtered. By turning off the filter in discontinuous regions, we turn off the ADM scheme (or the SSM part of the DMM) and allow the underlying shock-capturing scheme to handle the parts of the flow that are governed by gasdynamics. Ideally, the SCF confines a shock to the same number of grid points that the underlying shock-capturing scheme requires to resolve a shock in the absense of any turbulence modelling.

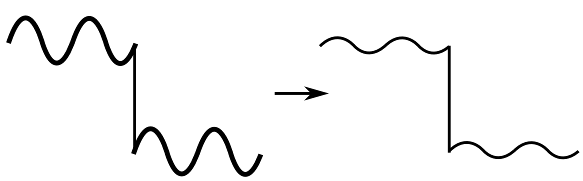

Figure 4. Ideal behavior of a shock-confining filter.

In order for the filter to adapt, its coefficients must be allowed to vary in space. We generalize the discrete filter definition from (55) to

$$\overline{f}_i = \sum_{k=-N}^{N} b_i^k f_{i+k} = \text{e.g.,}\ \ b_i^{-1} f_{i-1} + b_i^0 f_{i+0} + b_i^1 f_{i+1}. \tag{59}$$

The new subscript index refers to the grid point where the filtered value is to be calculated. The superscript continues to refer to the offset from that location. In smooth regions, the adaptation should turn off and the coefficients should reduce to their "optimal" or linear values $b_k^i = a_k$.

The WENO scheme for the convective fluxes uses a stencil built from a selection of candidate stencils around the point of interest with different biases. A measure of the degree of WENO stencil adaptation is provided by the nonlinearity index NI as given in Weirs[19] or Taylor et al.[20] Here we use the quantity that is referred to as NI' in Taylor et al.,[20] which is NI renormalized such that $NI' = 0$ indicates no adaptation, and $NI' = 1$ indicates a maximally adapted stencil. The WENO scheme adapts based on the smoothness of individual characteristic flow variables, but the SCF is applied to conserved variables. We therefore seek a single quantity that gives a measure of whether a shock exists at a particular location. If we are filtering in the x_i direction, then the NI' values corresponding to the three characteristic variables that would be involved in a shock or other discontinuity in that direction are averaged to give a value that we shall call a barrier height α. We call it a barrier height because we are notionally creating a barrier at each cell face to control the flow of information across discontinuities during filtering. The simulations actually use a finite difference code, but we will still talk in terms of cell faces in the context of SCF.

We constrain the filter adaptation to preserve two properties of the filter:

- P1–Global conservation of the variable, i.e.,

$$\sum_i \overline{f}_i = \sum_i f_i. \tag{60}$$

- P2–Preservation of constants, i.e.,

$$f_i = C,\ \forall\ i \in [a, b] \Longrightarrow \overline{f}_i = C,\ \forall\ i \in [a + N, b - N]. \tag{61}$$

In the derivation of the LES equations from the Navier-Stokes equations, we have assumed that filtering commutes with differentiation, i.e.,

$$\overline{\frac{\partial \phi}{\partial x}} = \frac{\partial \overline{\phi}}{\partial x}. \tag{62}$$

Unfortunately, this property cannot be maintained in regions of the flow where the filter is adapting. We assume that in high speed flows, the potential benefit from lessening oscillations near discontinuities outweighs the commutation error introduced by the adaptation. It follows easily from (59) that the filter is automatically linear in the sense that $\overline{a\phi + b\psi} = a\overline{\phi} + b\overline{\psi}$ for scalar constants a, b and functions ϕ, ψ. We also make repeated use of this fact throughout the derivation.

Consider a filter with a stencil covering the points $(i - 1, i, i + 1)$. For simplicity, assume a periodic domain of N_x points. Then the values b^i_k represent $3N_x$ degrees of freedom. Enforcing properties P1 and P2 imposes $2N_x$ constraints, leaving N_x degrees available for adaptation. As mentioned above, we choose to impose a barrier height $\alpha_{i+\frac{1}{2}}$ at each cell face $i + \frac{1}{2}$ such that $\alpha_{i+\frac{1}{2}} = 1$ totally prevents information from being referenced across that face and $\alpha_{i+\frac{1}{2}} = 0$ corresponds to uninhibited reference to such information. Imposing these barriers at each of the N_x cell faces makes use of the remaining degrees. Schematically, we can imagine information being partially reflected and transmitted at each cell face based on the local barrier height as in Figure 5. We can imagine an effective value of f_{i-1} that is used in calculating $\overline{f}_i$. Let $f^{\text{eff}}_{i-1,i}$ denote this effective value of f_{i-1} as "seen" from i. We choose a simple linear combination:

$$f^{\text{eff}}_{i-1,i} = (1 - \alpha_{i-1/2})f_{i-1} + \alpha_{i-1/2}f_i. \tag{63}$$

Similarly,

$$f^{\text{eff}}_{i+1,i} = (1 - \alpha_{i+1/2})f_{i+1} + \alpha_{i+1/2}f_i. \tag{64}$$

In cases of wider filter stencils, we continue to use a simple linear combination of two points, but we multiply the intervening transmission fractions: e.g.,

$$f^{\text{eff}}_{i+3,i} = (1 - \alpha_{i+\frac{5}{2}})(1 - \alpha_{i+\frac{3}{2}})(1 - \alpha_{i+\frac{1}{2}})f_{i+3} + [1 - (1 - \alpha_{i+\frac{5}{2}})(1 - \alpha_{i+\frac{3}{2}})(1 - \alpha_{i+\frac{1}{2}})]f_i. \tag{65}$$

The effective quantities are operated on using the linear filter coefficients:

$$\overline{f}_i = \sum_{k=-N}^{N} a^k f^{\text{eff}}_{i+k,i} = \sum_{k=-N}^{N} b_i^k f_{i+k}. \tag{66}$$

This expression can be solved for the adaptive stencil coefficients b_i^k. An adaptive filter derived in this manner automatically satisfies the desired properties P1 and P2.

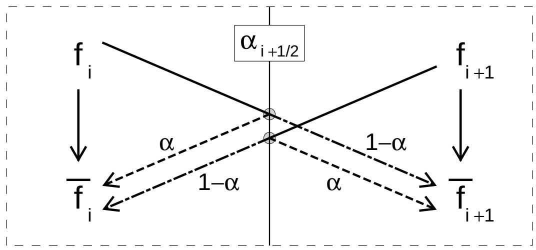

Figure 5. Notional transmission and reflection of information at a cell face barrier.

In the case of linear filters, a three-dimensional filter is often implemeneted using the successive application of one-dimensional filters in the Cartesian basis i-, j-, and k-directions. However, in the case of the SCF, the three-dimensional filter produced in this manner would depend on the order in which the three one-dimensional filters were applied. We would like the SCF to have no preferred direction, so we effectively average the six possible orders in which we could apply the i-, j-, and k-filters. Let us denote the filter operations in the i-, j-, and k-directions as $\overline{f}^{\,i}_{i,j,k}$, $\overline{f}^{\,j}_{i,j,k}$, and $\overline{f}^{\,k}_{i,j,k}$, respectively. We use a, b, and c to distinguish between the filter coefficients in the three directions, and we now use three subscripts to identify the grid point at which the filtered value is to be found:

$$\overline{f}^{\,i}_{i,j,k} = \sum_{\ell=-N}^{N} \left[a^{\ell}_{i,j,k}\right] f_{i+\ell,j,k} \tag{67}$$

$$\overline{f}^{\,j}_{i,j,k} = \sum_{m=-N}^{N} \left[b^{m}_{i,j,k}\right] f_{i,j+m,k} \tag{68}$$

$$\overline{f}^{\,k}_{i,j,k} = \sum_{n=-N}^{N} \left[c^{n}_{i,j,k}\right] f_{i,j,k+n} \tag{69}$$

Applying the filters in the order i, j, k results in the expression:

$$\overline{\overline{\overline{f}}}^{\,i,j,k}_{i,j,k} = \sum_{n=-N}^{N}\sum_{m=-N}^{N}\sum_{\ell=-N}^{N} \left[c^{n}_{i,j,k} b^{m}_{i,j,k+n} a^{\ell}_{i,j+m,k+n}\right] f_{i+\ell,j+m,k+n}. \tag{70}$$

The roles of the coefficients in the bracketed portion of (70) depend on the filtering order. In order to define a three-dimensional filter without such a dependence, we define new coefficients according to

$$\begin{aligned} d_{i,j,k,\ell,m,n} \equiv \frac{1}{6}\{ & c^{n}_{i,j,k} b^{m}_{i,j,k+n} a^{\ell}_{i,j+m,k+n} + c^{n}_{i,j,k} b^{m}_{i,j+m,k+n} a^{\ell}_{i,j+m,k} \\ & + c^{n}_{i+\ell,j+m,k} b^{m}_{i,j,k} a^{\ell}_{i,j+m,k} + c^{n}_{i,j+m,k} b^{m}_{i,j,n} a^{\ell}_{i,j+m,k+n} \\ & + c^{n}_{i+\ell,j,k} b^{m}_{i+\ell,j,k+n} a^{\ell}_{i,j,k} + c^{n}_{i+\ell,j+m,k} b^{m}_{i+\ell,j,k} a^{\ell}_{i,j,k} \} \end{aligned} \tag{71}$$

Then the filtered quantity is computed as

$$\overline{\overline{\overline{f}}}^{3D}_{i,j,k} = \sum_{n=-N}^{N} \sum_{m=-N}^{N} \sum_{\ell=-N}^{N} \left[d_{i,j,k,\ell,m,n}\right] f_{i+\ell,j+m,k+n}. \tag{72}$$

We drop the superscript $3D$ and return to using a single overbar for the remainder of the paper.

IV. Numerical Simulations

All simulations in this paper are computed using a finite difference code to solve the governing equations in conservative form. Unless stated otherwise, the convective terms are computed using a fourth-order-accurate bandwidth-optimized symmetric WENO scheme[19, 21, 22] that uses four points per candidate stencil. A relative limiter is applied to the WENO smoothness index in Taylor et al. in order to improve the grid convergence properties and to prevent WENO from erroneously adapting in regions containing only turbulent fluctuations. In cases where we use the relative smoothness limiter,[20] which we denote as WENO-RL, we use a value $\alpha_{\mathrm{RL}} = 10$ in the terminology of Taylor et al.[20] In the case of the ADM with relaxation regularization, we use eight-point fourth-order-accurate central differences that have been bandwidth-optimized. Time integration is carried out using a low-storage third-order-accurate Runge-Kutta scheme due to Williamson.[23] Modeled fluxes appearing on the right-hand sides of governing equations are computed using fourth-order central differences, as are the viscous terms.

IV.A. Shocktube

In order to decouple the effects of gasdynamics from those of turbulence, we first consider a shocktube problem. We choose a one-dimensional, periodic domain with 256 grid points and left and right initial states $(\rho_L, u_L, p_L) = (1\mathrm{kg/m}^3, 0\mathrm{m/s}, 1\mathrm{Pa})$ and $(\rho_R, u_R, p_R) = (0.1\mathrm{kg/m}^3, 0\mathrm{m/s}, 0.125\mathrm{Pa})$. At the start of the simulation, shocks, contact surfaces, and expansion waves form and propagate away from the interfaces between the left and right states. (Because of the symmetry of the problem, we only present results from half of the domain.) We stop the simulation before the physical waves interact, but numerical disturbances due to the ADM defiltering operation propagate faster than physical waves and do interact somewhat due to the periodic boundary condition. Other simulations with very long non-periodic domains suggest that the interaction does not qualitatively change the results.

Because the shocktube flow lacks turbulence and the corresponding range of lengthscales, a brief note is in order about terminology in this section. The terms DNS and LES (or ADM) refer to simulations using the same grid resolution; they do not correspond to simulations that resolve any particular fraction of turbulent kinetic energy or viscous dissipation. By DNS we refer to the solution of equation (1), and by ADM we refer to the solution of equation (33), with or without secondary regularization via a relaxation term or an SGS model.

All of the shocktube results plotted here were computed using the simple tophat filter (either linearly or in SCF form). The other two filters discussed in Section III give very similar results and are not plotted here.

Figure 6 plots the density profile along the shocktube. Spurious oscillations develop around discontinuities when using the ADM, both with and without regularization. The WENO shock-capturing method applied to a DNS (using the same grid) removes the oscillations; however, as shown in Figure 7, WENO applied to the ADM convective terms in equation (33) does not eliminate the oscillations for an ADM simulation. Figure 8 shows that the use of the shock-confining filter with ADM largely eliminates the oscillations; however, a qualitative change in the solution appears near one edge of the expansion wave. This anomaly is made worse by the use of relative smoothness limiters in the WENO-RL method, but it does not produce new extrema and seems to be more localized than the original spurious oscillations.

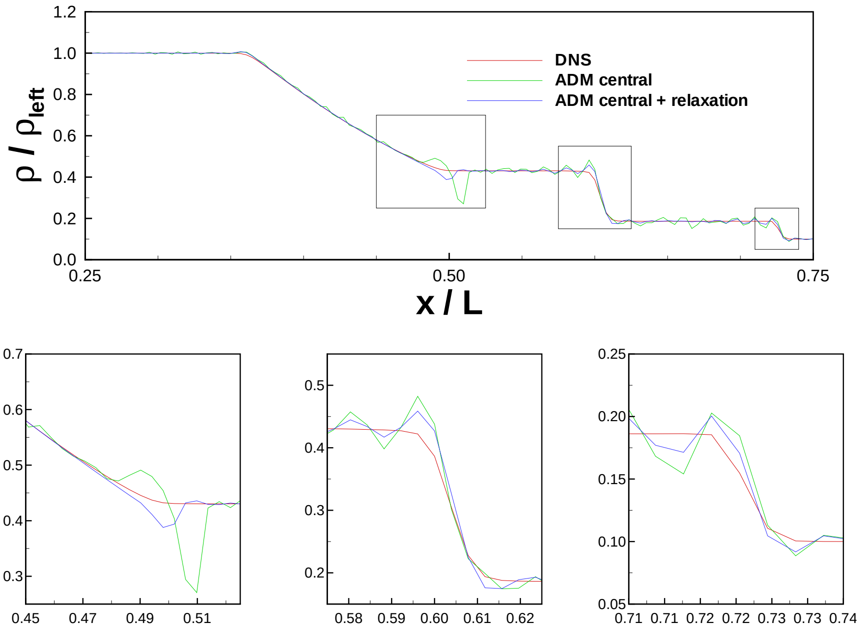

Figure 6. Density profiles in shocktube problem for WENO-based DNS, ADM with central differencing, and ADM with central differencing and relaxation regularization.

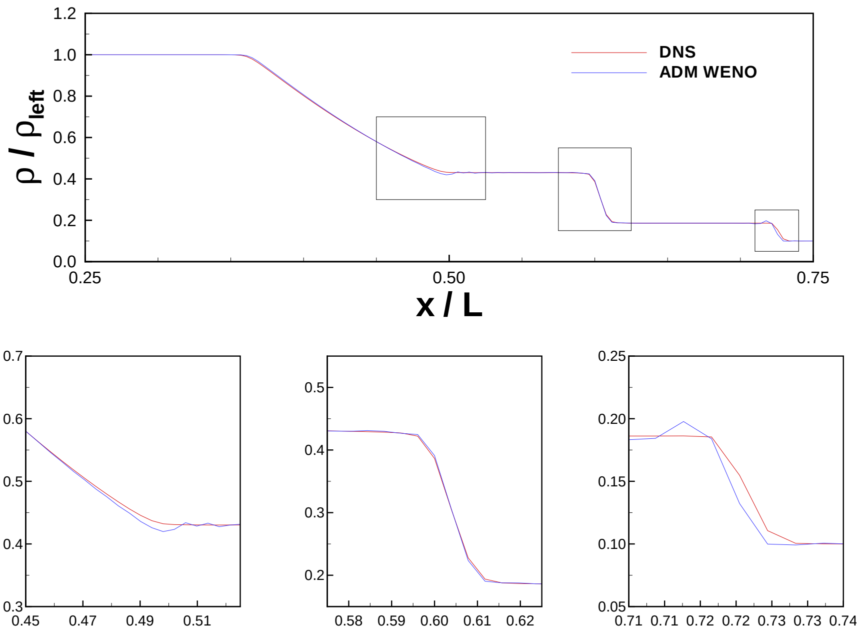

Figure 7. Density profiles in shocktube problem for WENO-based DNS and WENO-based ADM using a linear tophat filter.

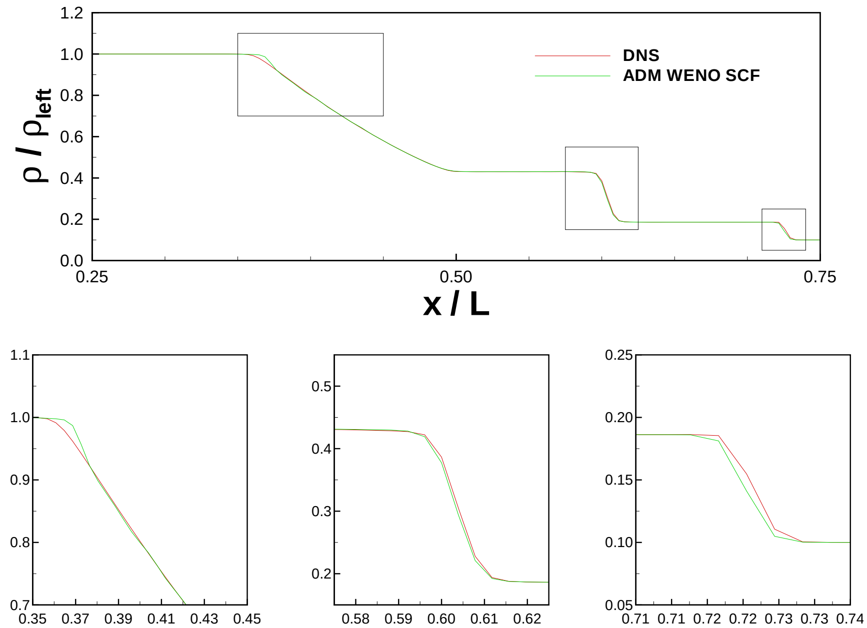

Figure 8. Density profiles in shocktube problem for WENO-based DNS and WENO- and WENO-RL-based ADM using a shock-confining tophat filter.

IV.B. Decaying Isotropic Turbulence

In order to assess the shock-confining filter in turbulent flows, we consider the problem of decaying compressible isotropic turbulence in a periodic box. We use a nominal initial Taylor microscale Reynolds number of $Re_\lambda = 50$ and nominal initial turbulent Mach numbers $M_t = q/a_{\text{avg}}$ of 0.3 and 0.9. In both cases, we compare the results from: the traditional DMM, the DMM using shock-confining filters, the ADM with dynamic relaxation, and the ADM with shock-confining filters and SGS model. All runs except for the ADM with relaxation use WENO-RL. The ADM with relaxation uses central differences following Stolz et al.[6,7] The filtered data from a DNS are included for reference. Note that the DNS data are filtered using a linear filter, and so the SCF results should not be expected to match perfectly. However, the traditional DMM and the ADM with relaxation should ideally approximate the linearly filtered DNS data. All filtering is done using the tophat filter.

The initial fields are advanced using DNS on 192^3 grid points until $t = 2u'_{\text{rms}}/\lambda$, at which time they are linearly filtered onto 48^3 grid points. At $t = 2u'_{\text{rms}}/\lambda$, the coarse grid resolves 75% and 74% of turbulent kinetic energy for the $M_t = 0.3$ and $M_t = 0.9$ cases, respectively.

The $M_t = 0.3$ case should contain almost no shocklets, and this case should give an indication of the suitability of the models for smooth turbulent flows. In Figure 9, the DMM with SCF and both ADMs show comparable behavior and good agreement with the rate of decay of turbulent kinetic energy. The traditional DMM is somewhat more dissipitive over a transient period of about $\Delta t = 2u'_{\text{rms}}/\lambda$, after which it appears to achieve a comparable decay rate with a persistent offset due to the initial transient.

Figure 10 shows the decay of root-mean-square temperature fluctuations with time, normalized by instantaneous volume-averaged temperature. The ADM with relaxation agrees well with the filtered DNS. The DMM with SCF and DMM with linear filtering both exhibit an initial period of greater attenuation followed by apparently correct dissipation rates with a persistent downward offset. The ADM with SCF is slightly more dissipative even after the initial transient period, but its decay curve remains comparable to the DMM curves until at least $t = 16u'_{\text{rms}}/\lambda$.

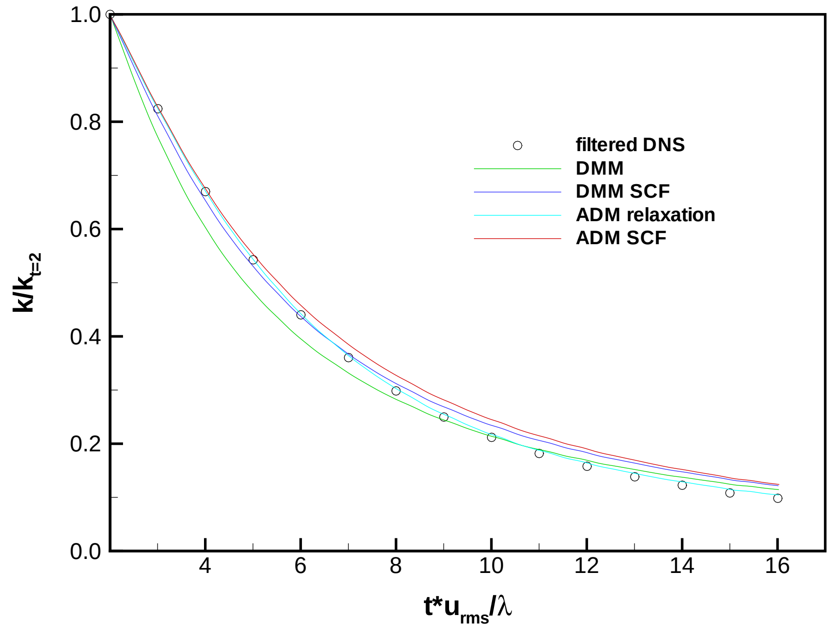

Figure 9. Decay of resolved turbulent kinetic energy for initial $Re_\lambda = 50$ and $M_t = 0.3$.

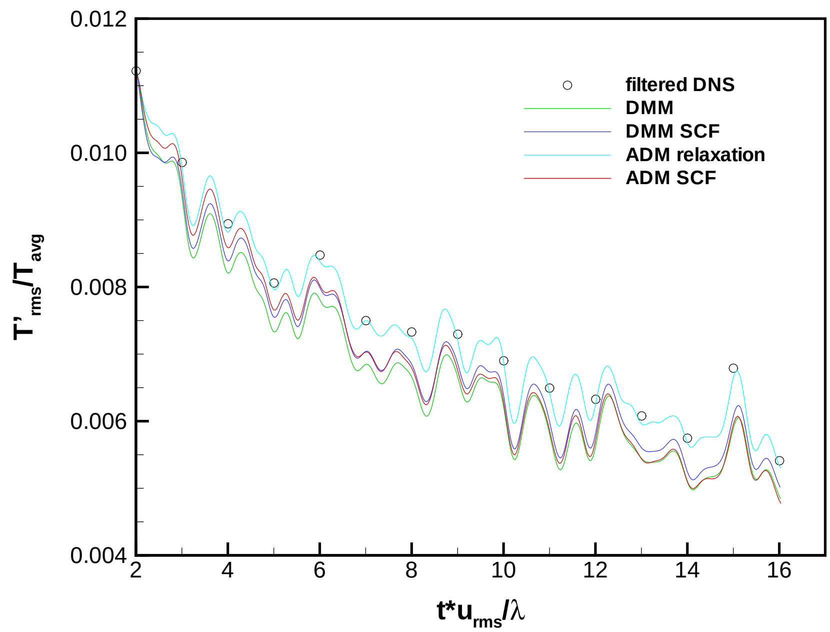

Figure 10. Decay of root mean square temperature fluctuations normalized by instantaneous average temperature for initial $Re_\lambda = 50$ and $M_t = 0.3$.

Figure 11 shows the energy spectra from the different models at $t = 4u'_{\text{rms}}/\lambda$, at which time the filtered DNS field resolves approximately 68% of the turbulent kinetic energy. All models studied show comparable spectra in the low wavenumber regions, but they all show significant attenuation compared to the filtered DNS. This may be due in part to numerical dissipation from the WENO-RL scheme in the DMMs and ADM with SCF. The ADM with relaxation shows a similar amount of attenuation for low wavenumbers but significantly greater attenuation at the highest wavenumbers, presumably because the relaxation term is active at these smallest scales.

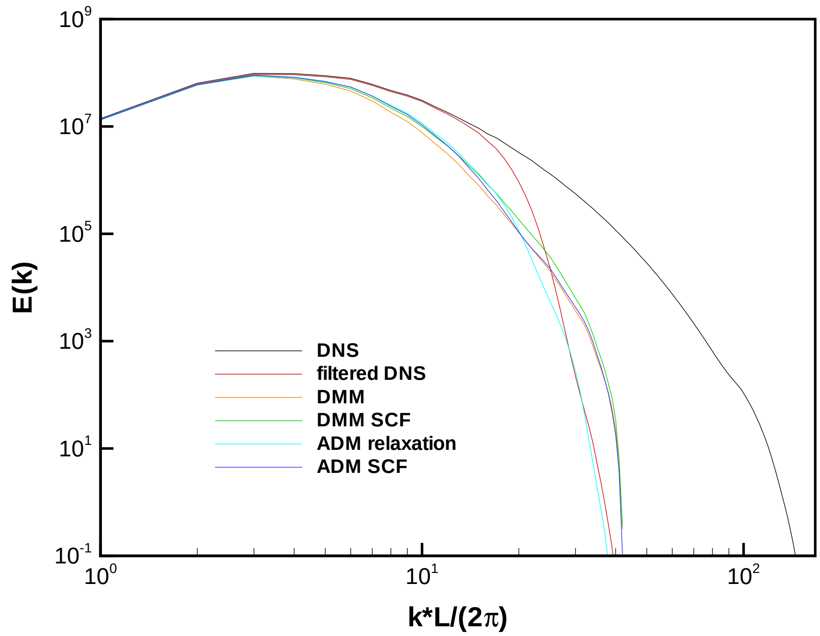

Figure 11. Energy spectra at $t = 4u'_{\text{rms}}/\lambda$ for initial $Re_\lambda = 50$ and $M_t = 0.3$.

Figure 12 shows the temperature spectra from the different models. As in the case of the energy spectra, all models studied show comparable temperature spectra in the low wavenumber regions, but they all show significant attenuation compared to the filtered DNS. Again, the ADM with relaxation shows greater attentuation at high wavenumbers.

The $M_t = 0.9$ case *does* contain significant shocklets, and this case should give an indication of the suitability of the models for flows that contain both smooth turbulent regions and shocks. In Figure 13, the models show trends similar to those for the $M_t = 0.3$. Namely, good agreement with the rate of decay of turbulent kinetic energy for all models except for the traditional DMM, which is somewhat more dissipitive over a transient period of about $\Delta t = 2u'_{\text{rms}}/\lambda$.

Figure 14 shows the decay of root-mean-square temperature fluctuations with time, normalized by instantaneous volume-averaged temperature. The ADM with relaxation agrees well with the filtered DNS. The other three models all exhibit an initial period of greater attenuation followed by apparently correct dissipation rates with a persistent downward offset. Unlike in the $M_t = 0.3$ case, the dissipation of temperature fluctuations is not significantly greater with the ADM and SCF than with the dynamic mixed models.

Figure 15 shows the energy spectra from the different models at $t = 4u'_{\text{rms}}/\lambda$, at which time the filtered DNS field resolves approximately 70% of the turbulent kinetic energy. All models show trends similar to those for the $M_t = 0.3$ case.

Figure 16 shows the temperature spectra from the different models. All models show trends similar to those in the energy spectra.

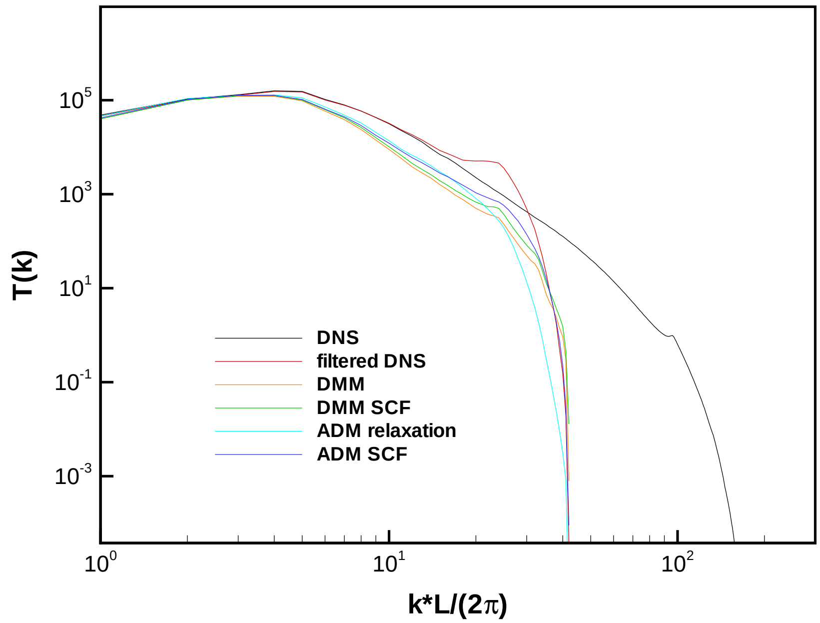

Figure 12. Temperature spectra at $t = 4u'_{\rm rms}/\lambda$ for initial $Re_\lambda = 50$ and $M_t = 0.3$.

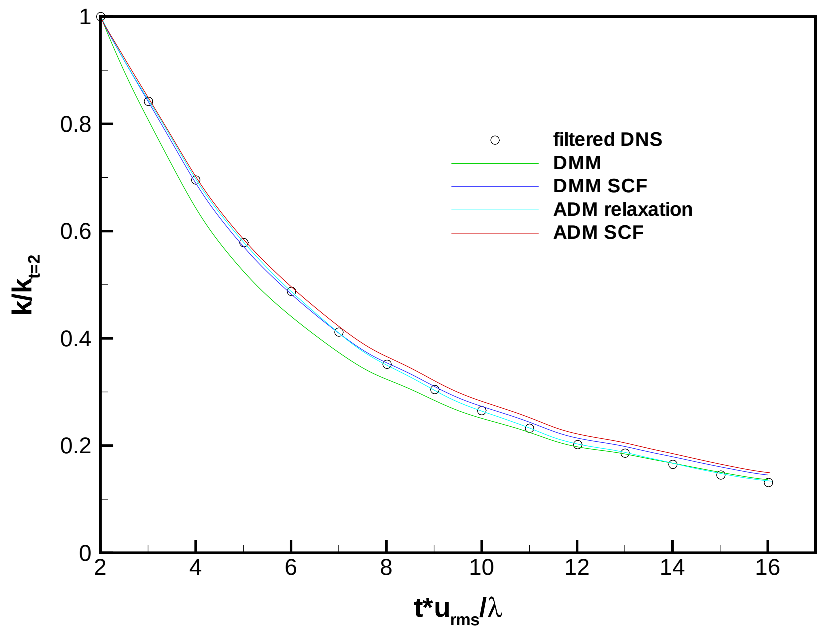

Figure 13. Decay of resolved turbulent kinetic energy for initial $Re_\lambda = 50$ and $M_t = 0.9$.

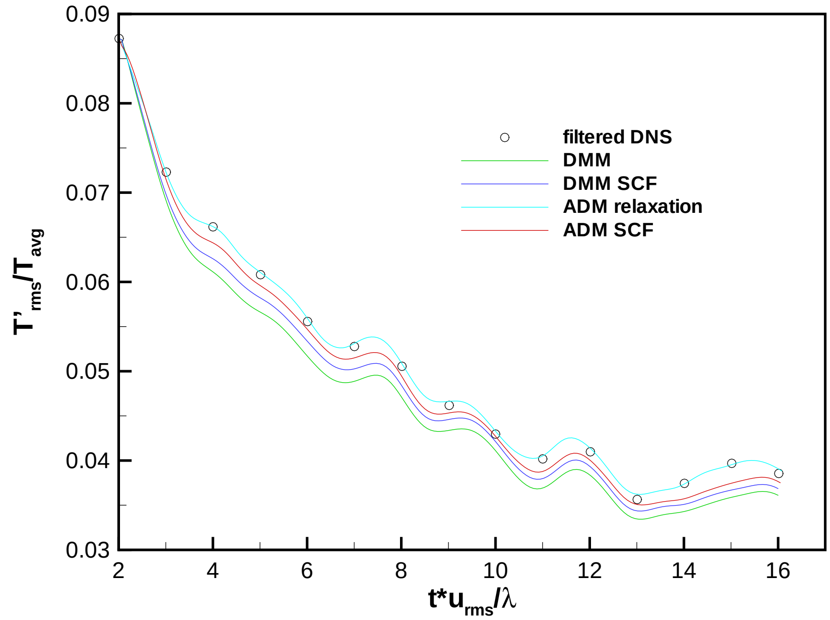

Figure 14. Decay of root mean square temperature fluctuations normalized by instantaneous average temperature for initial $Re_\lambda = 50$ and $M_t = 0.9$.

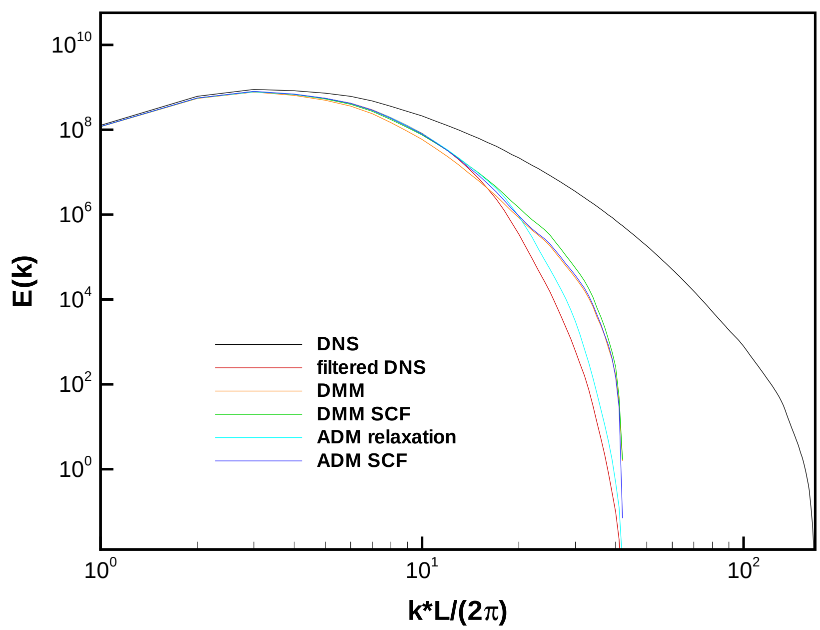

Figure 15. Energy spectra at $t = 4u'_{\rm rms}/\lambda$ for initial $Re_\lambda = 50$ and $M_t = 0.9$.

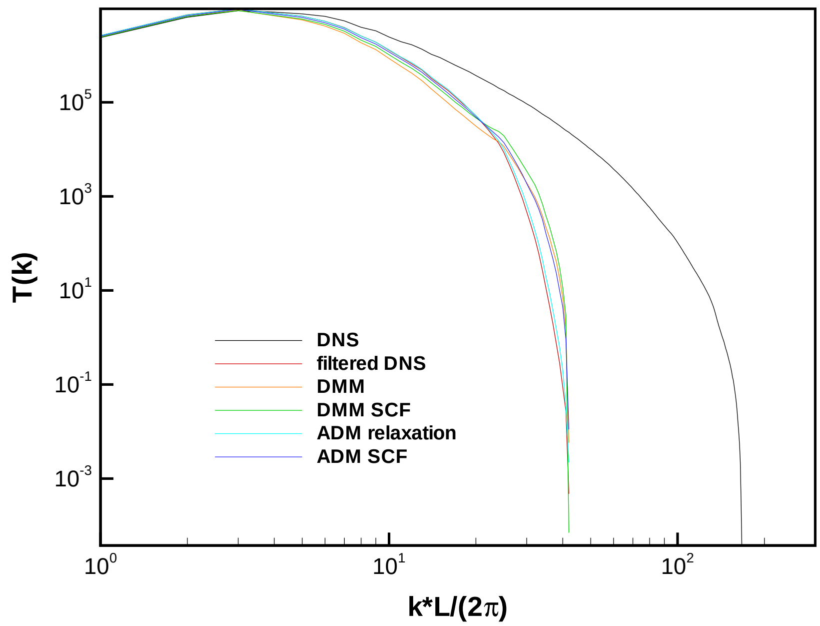

Figure 16. Temperature spectra at $t = 4u'_{\mathrm{rms}}/\lambda$ for initial $Re_\lambda = 50$ and $M_t = 0.9$.

To assess the importance of the SGS model relative to the numerical dissipation in smooth regions, we quantify the dissipation rates due to the SGS model, to viscosity, and to WENO adaptation in decaying isotropic turbulence under nearly incompressible conditions. We generate an initial field with nominal parameters $Re_\lambda = 50$ and $M_t = 0.1$ on a 192^3 grid. A DNS is computed until time $t = 2u'_{\mathrm{rms}}/\lambda$ to allow the development of realistic turbulence, and then the solution is filtered onto a 48^3 grid which resolves 74% of the turbulent kinetic energy. An ADM using WENO-RL and shock-confining filter is then run until $t = 4u'_{\mathrm{rms}}/\lambda$ to allow any transient effects of the grid coarsening to decay. At $t = 4u'_{\mathrm{rms}}/\lambda$, the LES field resolves 67% of the turbulent kinetic energy.

We assume that the contribution from the dissipation sources can be added to find the total: $\epsilon_{\mathrm{total}} = \epsilon_{\mathrm{visc}} + \epsilon_{\mathrm{numerical}} + \epsilon_{\mathrm{SGS}}$. The total dissipation $\epsilon_{\mathrm{total}}$ can be computed directly by comparing turbulent kinetic energy at successive timesteps. Repeating with and without viscous and SGS terms allows us to determine ϵ_{visc} and ϵ_{SGS}. Then we subtract to find the numerical dissipation $\epsilon_{\mathrm{numerical}}$. In this case, the SGS model accounts for 1% of the dissipation; WENO-RL, for 79%; and viscosity, for 20%. Thus, when used in conjunction with the WENO-RL method with $\alpha_{RL} = 10$, the SGS closure proposed for ADM provides negligible dissipation. However, the relative limiter value used here is intended for DNS, and its use has not yet been studied on coarser LES grids. A different limiter value more appropriate for LES might reduce the WENO adaptation (and $\epsilon_{\mathrm{numerical}}$) in this flow and result in a greater fraction of the dissipation being carried by the SGS model.

V. Conclusions

We have proposed a new shock-confining filtering method for LES of compressible flows that separates turbulent scales into resolved and unresolved parts but avoids filtering shocks and other discontinuities. Numerical simulations of the shocktube problem show that use of this new filter largely eliminates the spurious oscillations that appear in ADM simulations with relaxation, with the exception of an anomaly at the edge of the expansion fan.

Numerical simulations of decaying isotropic turbulence show that the use of the shock-confining filter with the dynamic mixed model reduces the excessive dissipation of the DMM during the initial transient period. The behavior of the DMM with SCF, and the ADM with SCF and SGS model are comparable. Although the ADM with relaxation gives somewhat better results in decaying turbulence, in problems with strong shocks such as shock/turbulent-boundary-layer interaction problems, it may be advantageous to accept the slightly inferior performance of the ADM with SCF or the DMM with SCF in order to avoid smearing of the strong shock and spurious oscillations in its vicinity.

Acknowledgments

This work is sponsored by the National Science Foundation under Grant CTS-0238390. Computational resources were provided by the CRoCCo Laboratory at Princeton University.

References

[1]Germano, M., Piomelli, U., Moin, P., and Cabot, W. H., "A dynamic subgrid-scale eddy viscosity model," *Phys. Fluids A*, Vol. 3(7), 1991, pp. 1760–1765.

[2]Lilly, D. K., "A proposed modification of the Germano subgrid-scale closure method," *Phys. Fluids A*, Vol. 4(3), March 1992, pp. 633–635.

[3]Bardina, J., Ferziger, J. H., and Reynolds, W. C., "Improved Subgrid Scale Models for Large Eddy Simulation," Aiaa paper 80–1357, Aug. 1980.

[4]Vreman, B., Geurts, B., and Kuerten, H., "On the formulation of the dynamic mixed subgrid-scale model," *Phys. Fluids*, Vol. 6(12), December 1994, pp. 4057–4059.

[5]Stolz, S. and Adams, N., "An approximate deconvolution procedure for large-eddy simulation," *Phys. Fluids*, Vol. 11(7), December 1999, pp. 1699–1701.

[6]Stolz, S., Adams, N. A., and Kleiser, L., "An approximate deconvolution model for large-eddy simulation with application to incompressible wall-bounded flows," *Phys. Fluids*, Vol. 13(4), 2001, pp. 997–1015.

[7]Stolz, S., Adams, N. A., and Kleiser, L., "The approximate deconvolution model for large-eddy simulations of compressible flows and its application to shock-turbulent-boundary-layer interaction," *Phys. Fluids*, Vol. 13(10), 2001, pp. 2985–3001.

[8]Harten, A., Engquist, B., Osher, S., and Chakravarthy, S. R., "Uniformly High Order Accurate Essentially Non-Oscillatory Schemes III," *Journal of Computational Physics*, Vol. 71, No. 2, 1987, pp. 231–303.

[9]Shu, C.-W. and Osher, S., "Efficient Implementation of Essentially Non-Oscillatory Shock-Capturing Schemes II," *Journal of Computational Physics*, Vol. 83, No. 1, 1989, pp. 32–78.

[10]Liu, X.-D., Osher, S., and Chan, T., "Weighted Essentially Non-Oscillatory Schemes," *Journal of Computational Physics*, Vol. 115, No. 1, 1994, pp. 200–12.

[11]Jiang, J.-S. and Shu, C.-W., "Efficient Implementation of Weighted ENO Schemes," *Journal of Computational Physics*, Vol. 126(1), 1996, pp. 202–228.

[12]Taylor, E. M., Grube, N. E., and Martín, M. P., "Evaluation of Traditional and Shock-Confining LES Filters using DNS Data of Compressible Turbulence," Aiaa paper 2007–4197, June 2007.

[13]Martín, M. P., Piomelli, U., and Candler, G. V., "Subgrid-Scale Models for Compressible Large-Eddy Simulations," *Phys. Fluids*, Vol. 13(11), November 2001, pp. 3400–3410.

[14]Smagorinsky, J., "General circulation experiments with the primitive equations: I. The basic experiment." *Mon. Weather Rev.*, Vol. 91, 1963, pp. 99–164.

[15]Moin, P., Squires, K., Cabot, W., and Lee, S., "A dynamic subgrid-scale model for compressible turbulence and scalar transport," *Phys. Fluids A*, Vol. 3(11), 1991, pp. 2746–2757.

[16]Speziale, C. G., Erlebacher, G., Zang, T. A., and Hussaini, M. Y., "The subgrid-scale modeling of compressible turbulence," *Phys. Fluids*, Vol. 31(4), 1988, pp. 940–942.

[17]van Cittert, P. H., "Zum Einfluß der Spaltbreite auf die Intensitatsverteilung in Spektrallinien II," *Zeitschrift für Physik*, Vol. 69, 1931, pp. 298–308.

[18]Vasilyev, O. V., Lund, T. S., and Moin, P., "A General Class of Commutative Filters for LES in Complex Geometries," *J. Comp. Phys.*, Vol. 46, 1998, pp. 82–104.

[19]Weirs, V. G., "A Numerical Method for the Direct Simulation of Compressible Turbulence," *Ph.D. thesis, University of Minnesota*, December 1998.

[20]Taylor, E. M., Wu, M., and Martín, M. P., "Optimization of Nonlinear Error for Weighted Essentially Non-Oscillatory Methods in Direct Numerical Simulations of Compressible Turbulence," *Journal of Computational Physics*, in press as of November 2006.

[21] Weirs, V. G. and Candler, G. V., "Optimization of weighted ENO schemes for DNS of compressible turbulence," Aiaa paper 1997–1940, 1997.

[22] Martín, M. P., Taylor, E. M., Wu, M., and Weirs, V. G., "A Bandwidth-Optimized WENO Scheme for the Direct Numerical Simulation of Compressible Turbulence," *Journal of Computational Physics*, Vol. 220(1), 2006, pp. 270–289.

[23] Williamson, J. H., "Low-storage Runge-Kutta Schemes," *Journal of Computational Physics*, Vol. 35, No. 1, 1980, pp. 48–56.